The local magnetic field scaling of gyrokinetic turbulence and its impact on tokamak transport

G. M. Staebler[1], J. Candy[1], E. Belli[1], J. E. Kinsey[2], N. Bonanomi[3],
J. Citrin[4], P. Mantica[5], R. E. Waltz[1], and JET Contributors[6]

[1] *General Atomics, San Diego, USA*

[2] *CompX, San Diego, USA*

[3] *IPP, Garching, Germany*

[4] *DIFFER, Eindoven, Netherlands*

[5] *ISTP-CNR, Milano, Italy*

[6] *See the author list of Ref. [1]*

Introduction

Gyrokinetic turbulence simulations with the CGYRO [2] and GENE [3] codes were performed in order to investigate the dependence of the turbulent transport on magnetic flux surface geometry. The 3-D saturated electric potential fluctuation intensity spectrum and the overall changes in the energy fluxes were examined to determine the dependence on the elongation and Shafranov shift of flux surfaces. A new saturation model, used in a quasi-linear evaluation of the fluxes, is able to reproduce the gyrokinetic fluxes well [4]. The verification and calibration of this model with a large database of CGYRO turbulence simulations is presented in Ref. [5].

Magnetic geometry of the gyrokinetic equation

The geometric metrics that enter the gyrokinetic equation for general, axisymmetric, closed flux surface geometry will be shown in this paper to provide the functions that fit the poloidal dependence of the saturated potential intensity. Because the gyroradius sets the scale for the plasma turbulence described by gyrokinetics, the wavelength perpendicular to the magnetic field is much shorter than the wavelength parallel to the magnetic field. This property makes it convenient to introduce an eikonal approximation for the perpendicular wavevector. The gradient of the eikonal (S) is perpendicular to the magnetic field vector $\mathbf{B}$: $\mathbf{B}\cdot\nabla S = 0$. There are two independent functions that satisfy this constraint. An arbitrary function of the poloidal flux $S = S_x(\psi)$ and $S = n\left[\varphi + S_y\right]$ where n is a toroidal mode index. The gyro-averaging operator (Bessel functions) have the argument $\left|\nabla S\right| v_\perp m_a c/(Z_a e B)$. This motivates defining a poloidally varying ion wavevector given by (see Ref.[2] for coordinate definitions)

$$K_{i\perp}^2 = \rho_{iB}^2\left|\nabla S\right|^2 = \left[K_{iy}^2 + \left(\hat{s}K_{iy}\Theta + K_{ix}\right)^2\right] \quad (1)$$

Where $\rho_{iB} = \sqrt{2T_i/m_i}/\Omega_B$, $\Omega_B = \frac{Z_i eB}{m_i c}$ are a gyro-radius and gyro-frequency using the ion temperature, mass and charge (T_i,m_i,Z_i) and using the total magnetic field magnitude $B(\theta)$. The magnetic shear is $\hat{s} = (r/q)dq/dr$. The generalized poloidal angle Θ in Eq. 1 is defined to be zero at the outboard midplane and has a quasi-periodic property derived from S_y. The poloidal K_{iy} and radial K_{ix} wavenumber components in Eq. 1 are defined by

$$K_{iy}(\theta) = \frac{n\rho_{iB_p}}{R} = \frac{k_y \alpha_i}{|\nabla r|}, K_{ix}(\theta) = |\nabla r| k_r \rho_{iB} = \frac{k_x \alpha_i}{G_q} \frac{B_{\text{norm}}}{B_{\text{unit}}}, G_q = \frac{rB}{qRB_p} = \frac{B}{B_{\text{unit}}|\nabla r|} \quad (2)$$

where the factor $\alpha_i = Z_{\text{norm}}\sqrt{m_i 2T_i}/(Z_i\sqrt{m_{\text{norm}}T_{\text{norm}}})$ converts from the arbitrary external normalizations used in k_y ($Z_{norm}, m_{norm}, T_{norm}$) to the ion values. The flux surface shape factor G_q has been introduced to highlight the distinction between the arbitrary normalizing magnetic field B_{norm} and B_{unit}, which appears in the metric coefficients. The poloidal wavenumber K_{iy} (Eq. 2) is the toridal wavenumber n/R normalized by the ion gyroradius with respect to the poloidal magnetic field $\rho_{iB_p} = \rho_{iB}B/B_p$. The radial ion wavenumber K_{ix} (Eq. 2) is the gradient normal to flux surfaces ($|\nabla r|k_r = |\nabla S_x|$) normalized to the the total magnetic field ion gyro-radius. Hence, the full magnetic field gyroradius sets the radial wavelength scale.

3-D saturated electric potential fluctuation intensity

The 3-D model [4] for the saturated electric potential fluctuation amplitude ($\Phi(\theta)_{k_x,k_y} = ae|\tilde{\phi}(\theta)_{k_x,k_y}|/T_e\rho_s\Delta K_{iy}$) (in CGYRO units) has the functional form

$$\Phi(\theta)_{k_x,k_y} = \frac{\Phi(\theta)_{0,k_y}}{(1+(k_x/k_x^{RMS})^2)} \quad (3)$$

This form approximates the observed CGYRO spectrum. Here it is assumed that the peak of the spectrum $\Phi(\theta)_{0,k_y}$ is at $k_x = 0$, which is true for the cases in this database. Note that the normalization of the fluctuation of the electric potential divides by the gyrokinetic expansion parameter ρ_s/a because the fluctuations are first order in this parameter (delta-f ordering). A model of the RMS width ($k_x^{\text{model}} \approx k_x^{RMS}|_{\theta=0}$) is given in Ref. [4]. The RMS width of the radial mode number spectrum (k_x^{RMS}) is computed at the outboard midplane ($\theta = 0$) by fitting the Lorentzian model distribution (Eq. 3) to the non-linear spectrum. The effective non-linear mixing rate defined by

$$\gamma_{k_y}^{\text{eff}} = k_x^{RMS} k_y \Phi(0)_{0,k_y} \quad (4)$$

is also computed directly from the non-linear spectrum at the outboard midplane ($\theta = 0$) . This has the dimensions of the non-linear ExB advection rate due to the finite k_y modes. The model for the effective mixing rate ($G(0)\gamma_{k_y}^{\text{model}} \approx \gamma_{k_y}^{\text{eff}}$) is given in Ref. [4]. All of the poloidal angle (θ) dependence is absorbed into the factor $G(\theta)$ that is fit to the amplitude of the peak potential

fluctuation spectrum at $k_x = 0$: $G(\theta) \approx \Phi(\theta)_{0,k_y}/\Phi(0)_{0,k_y}$. The model for the shape function is

$$\begin{aligned} G^2(\theta) &= d_1 G_1(\theta) \text{ for } k_y < k_{\text{ycut}} \\ &= \Big(d_1 G_1(\theta) k_{\text{ycut}} + b_3 d_2 G_2(\theta)(k_y - k_{\text{ycut}})\Big)/k_y \text{ for } k_y \geq k_{\text{ycut}} \end{aligned} \tag{5}$$

where $b_3 = 2.4$ and the coefficients k_{ycut}, d_1, d_2 are independent of θ [4]. The two geometric shape functions are:

$$G_1 = \Big(\frac{B(0)}{B(\theta)}\Big)^4, G_2 = \Big(\frac{G_q(0)}{G_q(\theta)}\Big)^4 \tag{6}$$

The saturated quasi-linear intensity ($I_{k_y}^{\text{model}}$) needed to evaluate quasi-linear fluxes is the flux surface average ($<>_\theta$) of the 3-D potential model (Eq. 3) evaluated at its peak at $k_x = 0$.

$$I_{k_y}^{\text{model}} = \Big\langle G^2(\theta) \Big\rangle_\theta \Big(\frac{\gamma_{k_y}^{\text{model}}}{k_x^{\text{model}} k_y}\Big)^2 \tag{7}$$

The reader is referred to Ref. [4] for the details of this new SAT2 saturation model.

Magnetic geometry dependence of turbulent fluxes

The quasi-linear fluxes computed using this new model (SAT2) for the quasi-linear intensity

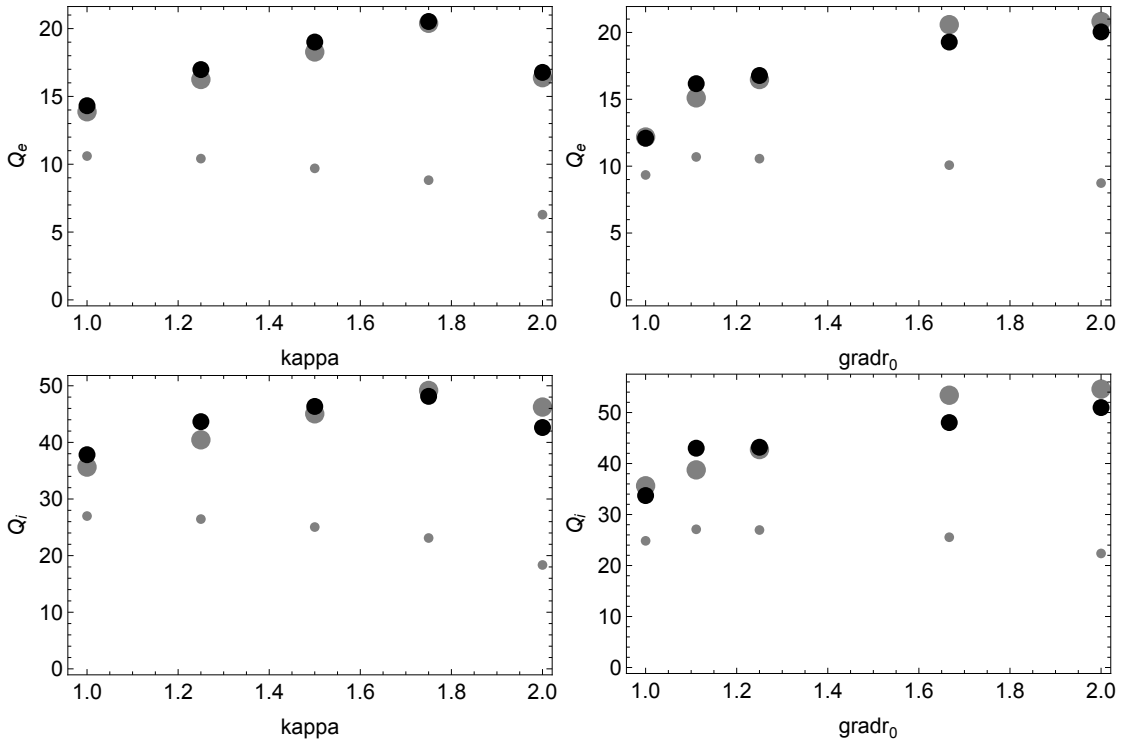

Figure 1: The total electron (top) and ion (bottom) energy fluxes for a κ scan (left) and a $\text{gradr}_0 = 1/(1 + dR/dr)$ scan (right) for CGYRO (black), SAT2 model (large gray) [4] and the previous SAT1 model (small gray)[6]

(Eq. 7), and the quasi-linear flux weights from linear CGYRO calculations of the most unstable

eigenmode, are compared to the non-linear CGYRO electron and ion energy fluxes in Fig. 1. The elongation (kappa) and Shavranov shift (dR/dr) of the flux surface were varied. Note that the fluxes in Fig. 1 use the CGYRO units with B_{unit} as the normalization for the magnetic field, which increases with elongation. The de-normalized physical flux for SAT2 still goes down with elongation just not as strongly as SAT1. Preliminary validation of the SAT2 model finds that the temperature and density predictions in the edge region of L-mode discharges is greatly improved. The shortfall of transport [7] in the outer 20% of the flux surfaces, that resulted in steep temperature gradients with TGLF with earlier saturation models, is eliminated with the SAT2 model for the limited number of DIII-D cases tested.

Acknowledgements

This material is based upon work supported by the U.S. Department of Energy, Office of Science, Office of Fusion Energy Sciences, using the DIII-D National Fusion Facility, a DOE Office of Science user facility, under Awards DE-SC0019736, DE-SC0018990, DE-FG02-95ER54309, and DE-FC02-04ER54698. This work has been carried out within the framework of the EUROfusion Consortium and has received funding from the Euratom research and training programme 2014-2018 and 2019-2020 under grant agreement No 633053. This work was supported by the Engineering and Physical Sciences Research Council [EP/L01663X/1]. We acknowledge the CINECA award under the ISCRA initiative, for the availability of high performance computing resources and support. Computing resources were provided by the Oak Ridge Leadership Computing Facility under Contract DE-AC05-00OR22725 and the National Energy Research Scientific Computing Center under Contract DE-AC02-05CH11231.

References

[1] Mailloux J 2021 *Nuclear Fusion* **Special issue 28th Fusion Energy Conference (Nice, France, 10-15 May 2021)** to be published

[2] Candy J, Belli E and Bravenec R 2016 *Journal of Computational Physics* **324** 73 – 93 ISSN 0021-9991

[3] Jenko F, Dorland W, Kotschenreuther M and Rogers B 2000 *Phys. Plasmas* **7** 1904

[4] Staebler G, Candy J, Belli E, Kinsey J E, Bonanomi N and Patel B 2020 *Plasma Phys. Control. Fusion* **63** 015013

[5] Staebler G 2021 *Nucl. Fusion* **submitted**

[6] Staebler G, Candy J, Howard N T and Holland C 2016 *Phys. Plasmas* **23** 062518

[7] Kinsey J E, Staebler G M, Candy J, Petty C C, Rhodes T L and Waltz R E 2015 *Phys. Plasmas* **22** 012507